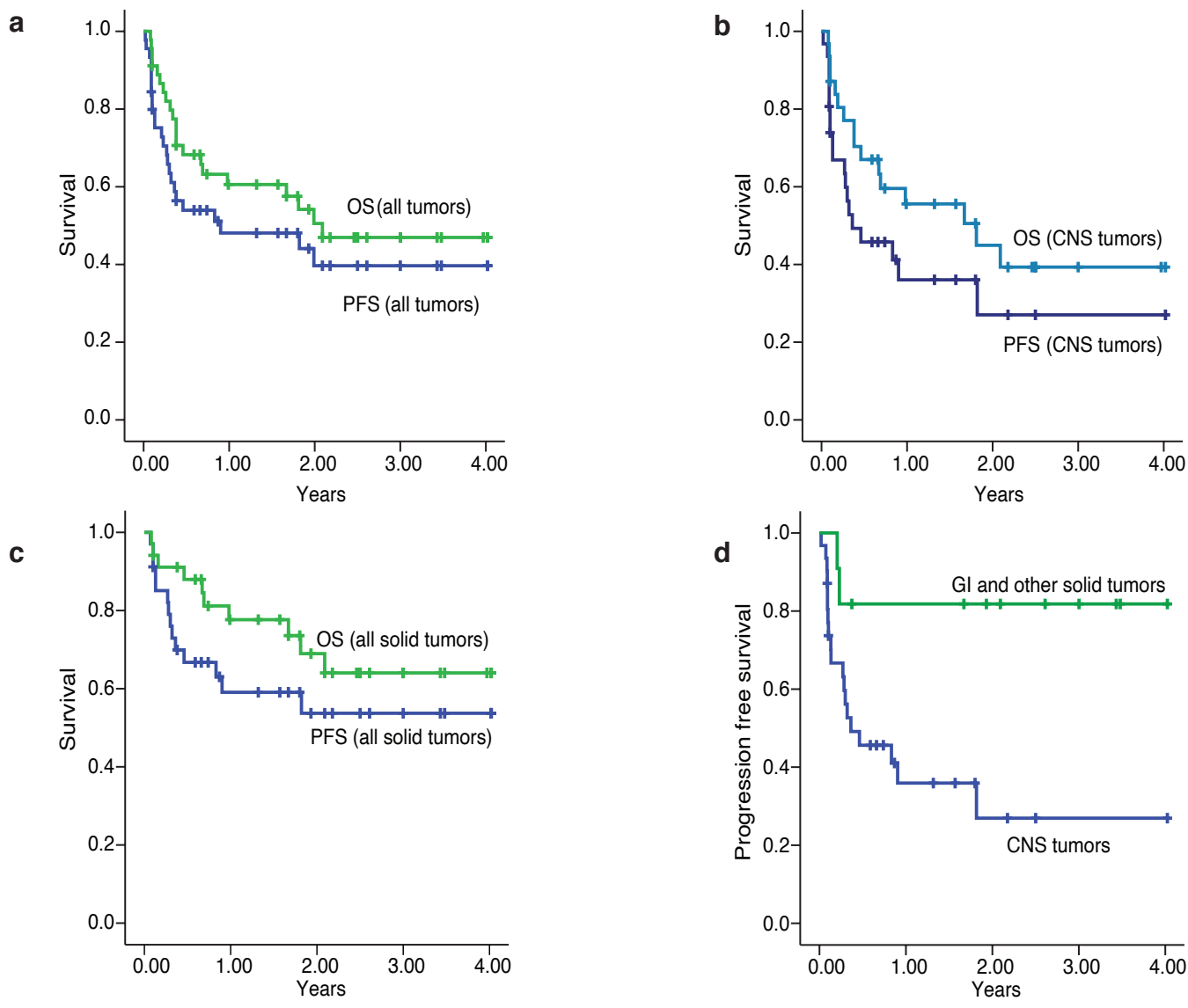


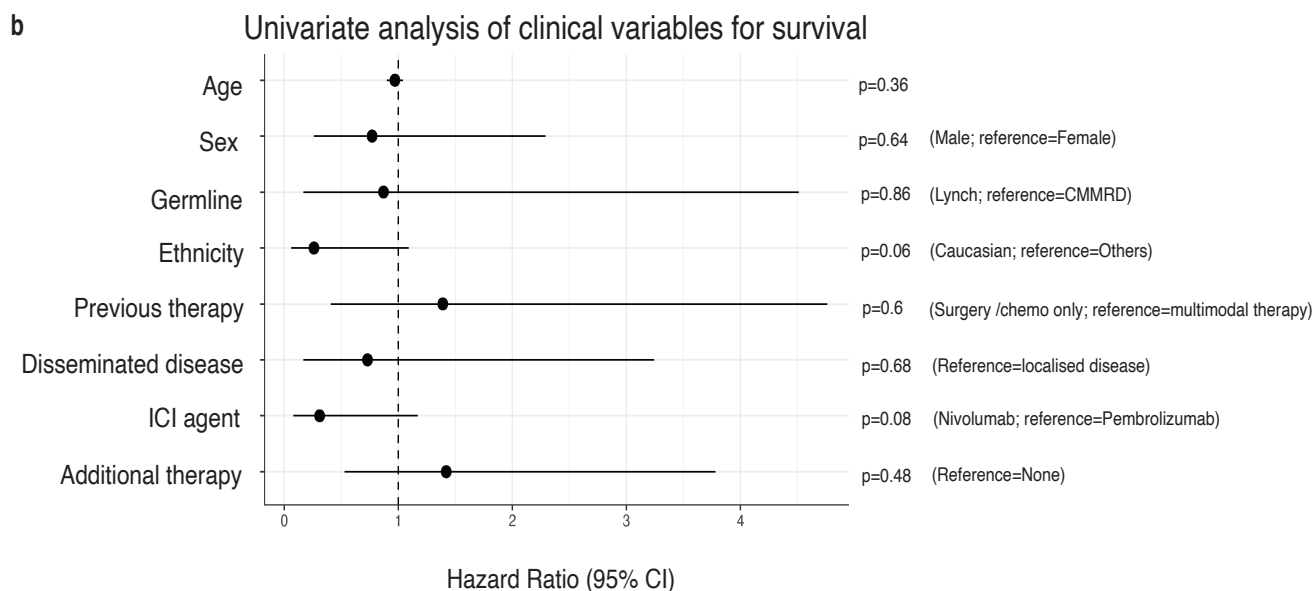
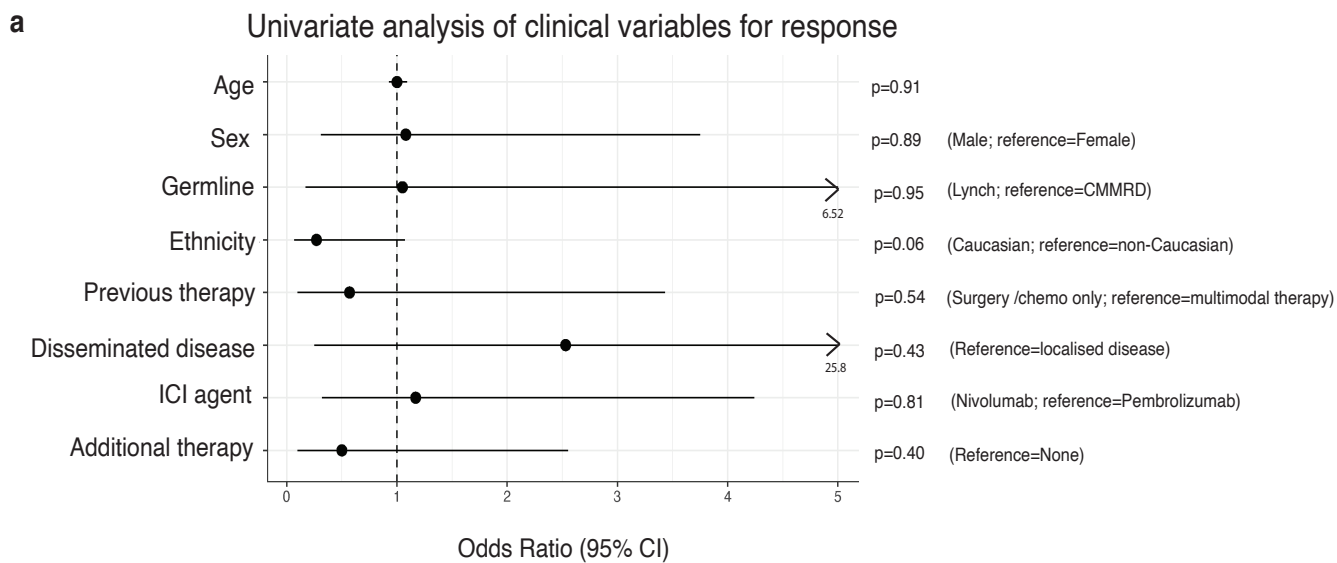
Supplementary information

Genomic predictors of response to PD-1 inhibition in children with germline DNA replication repair deficiency

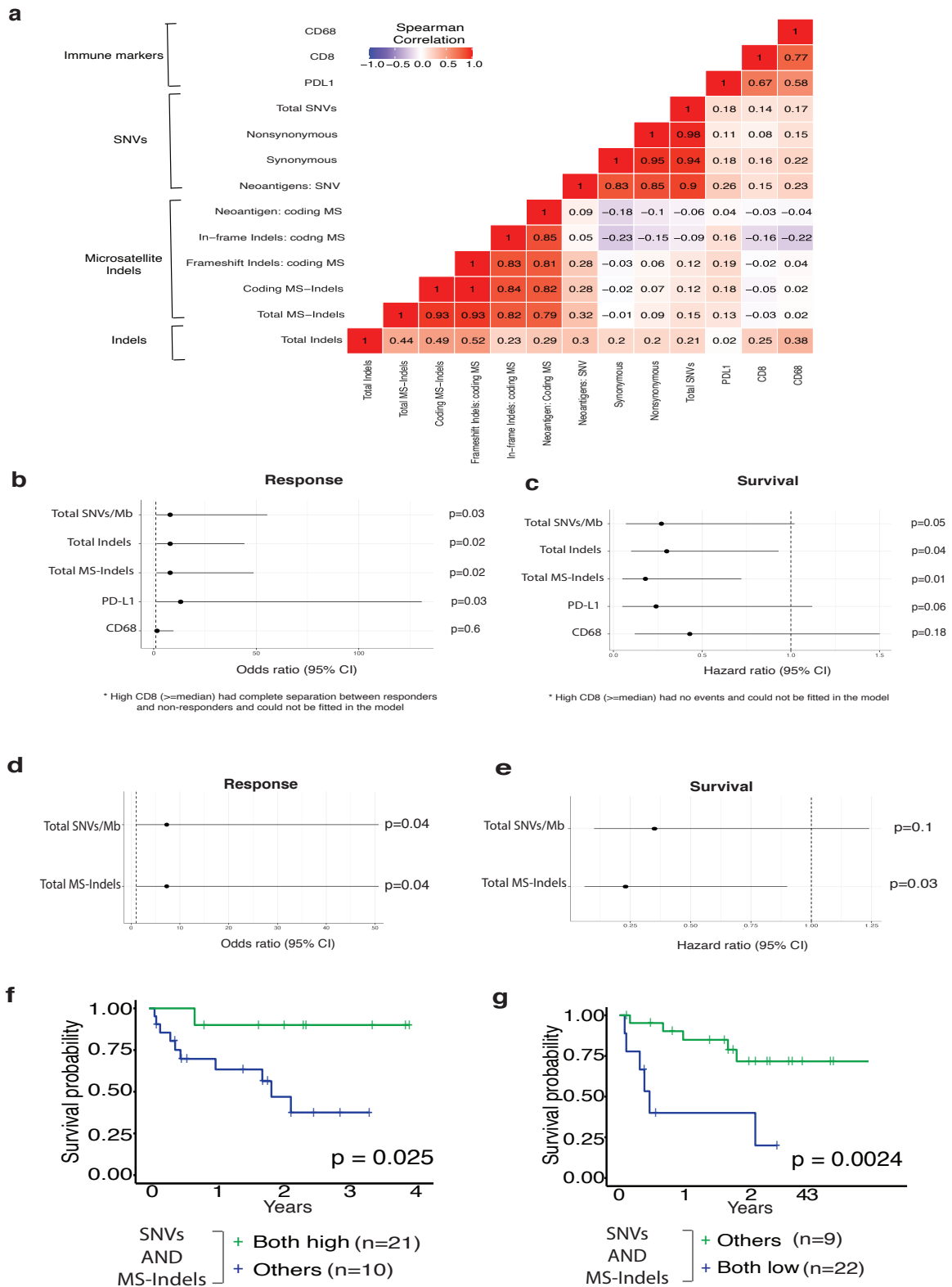
In the format provided by the authors and unedited



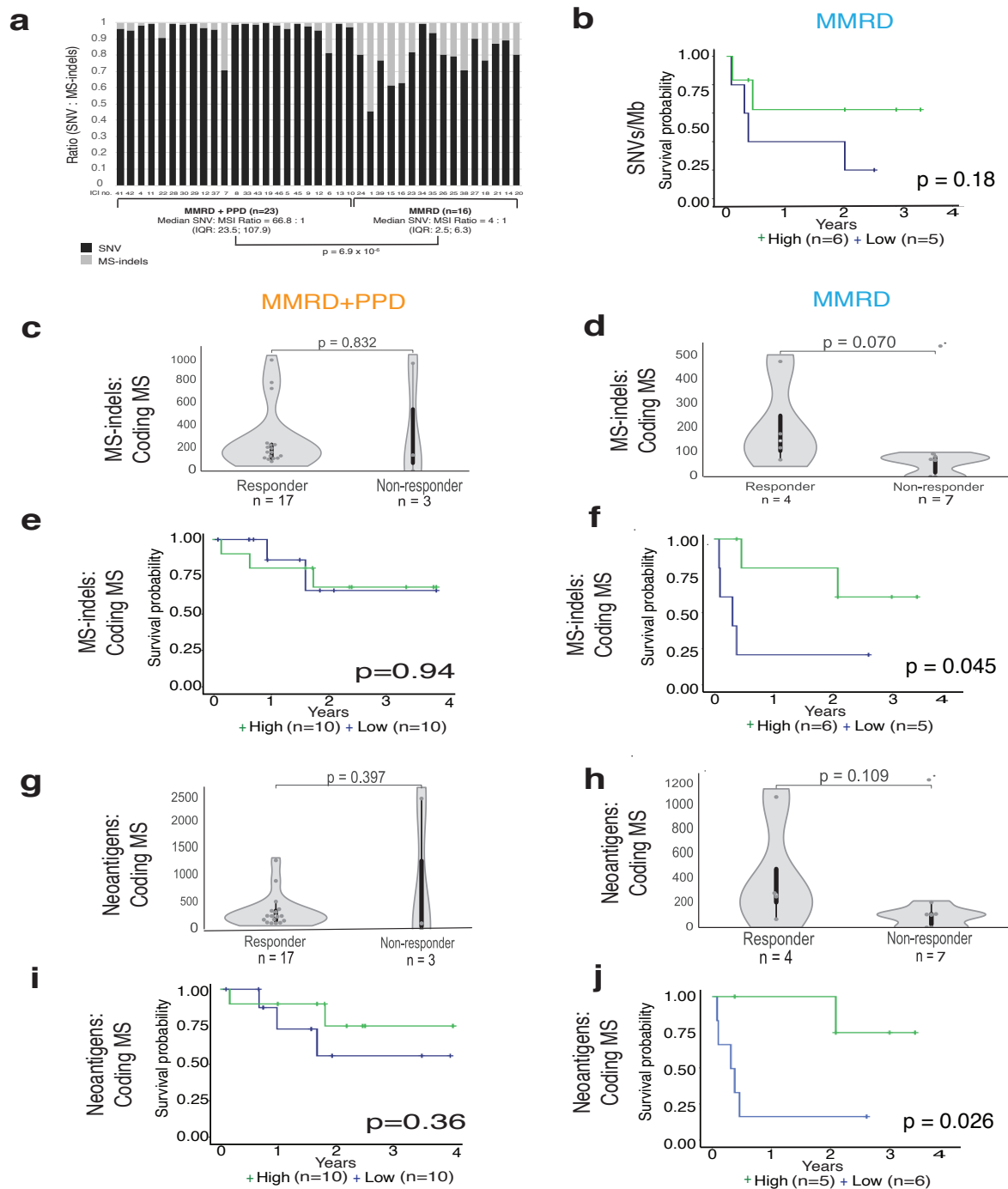
Supplementary Fig.S1. KM estimates of progression-free and overall survival for **(a)** all tumours, **(b)** CNS tumours, **(c)** all solid tumours (CNS and non-CNS). **(d)** Progression free survival for non-CNS solid tumours versus CNS tumours ($p=0.01$; 2-sided). The log-rank test was used to compare between the groups.



Supplementary Fig.S2. Univariable analysis of clinical predictors for **(a)** response and **(b)** survival following ICI at recurrence for replication-repair deficient cancers. Univariable logistic regression, estimated through generalized estimating equations, was fitted to assess association between each clinical variable and response. Univariable Cox regression model with robust standard errors was fitted to assess association between each clinical variable and survival. All p-values are 2-sided.

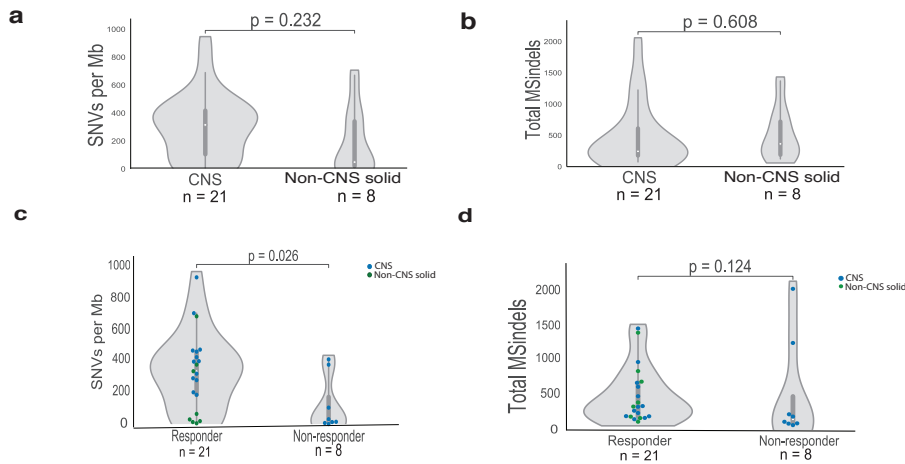


Supplementary Fig.S3. Biomarkers for response to ICI in replication-repair deficient cancers. (a) Spearman's rank correlation coefficient for dependent and independent variables. (b, c) Effects size (95% confidence intervals) for univariable analyses for the independent predictors for (b) response (assessed using univariable logistic regression) and (c) survival (assessed using univariable Cox regression model). (d-g) Dual role of SNVs and MS-indels in predicting outcomes: Multivariable analyses for (d) response (using logistic regression) and (e) survival (using Cox regression model) showing effects size and 95% confidence intervals. Kaplan-Meier (KM) curves for tumors with (f) both high and (g) both low SNVs and MS-indels (cut offs at the median values). All p-values are 2-sided.

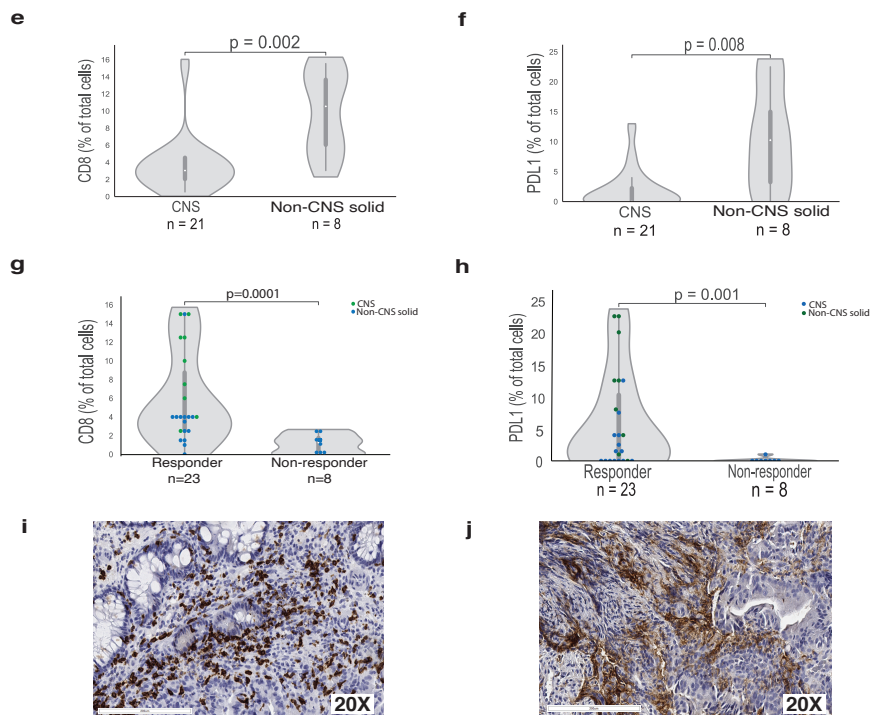


Supplementary Fig.S4. (a) SNVs outnumber MS-indels in tumors with MMRD+PPD (Wilcoxon-Mann-Whitney test). Each bar represents the SNV count (black) and MS-indel (grey) for each individual tumor with identifiers mentioned on the x-axis. **(b)** Overall survival for MMRD tumors by SNVs/Mb (\geq median). **(c-f)** Response and survival for MS-indels in coding microsatellites in MMRD+PPD versus MMRD tumors. **(g-h)** Response and survival for neoantigens generated by MS-indels in coding microsatellites in MMRD+PPD versus MMRD tumors. For survival, median values were utilized to stratify into 'high' and 'low' groups. For all box-plots for responders and non-responders, data are represented as median \pm interquartile range. For statistical significance in comparing responders and non-responders, the Wilcoxon-Mann-Whitney test was used. Survival analysis was performed using the Kaplan-Meier method, and the log-rank test was used to compare groups. All p values are 2-sided.

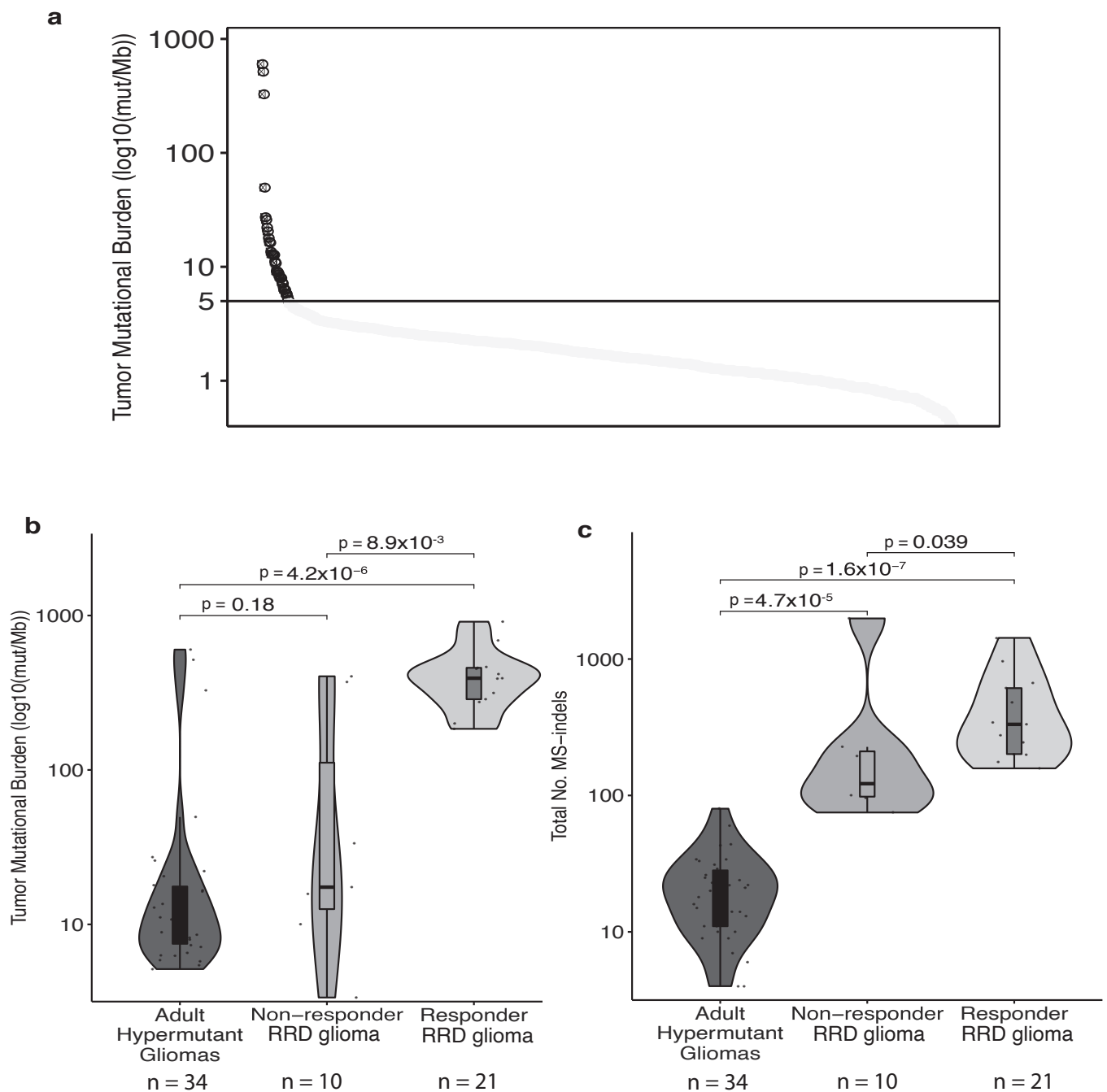
Predictive Genomic Biomarkers



Predictive Immune Biomarkers

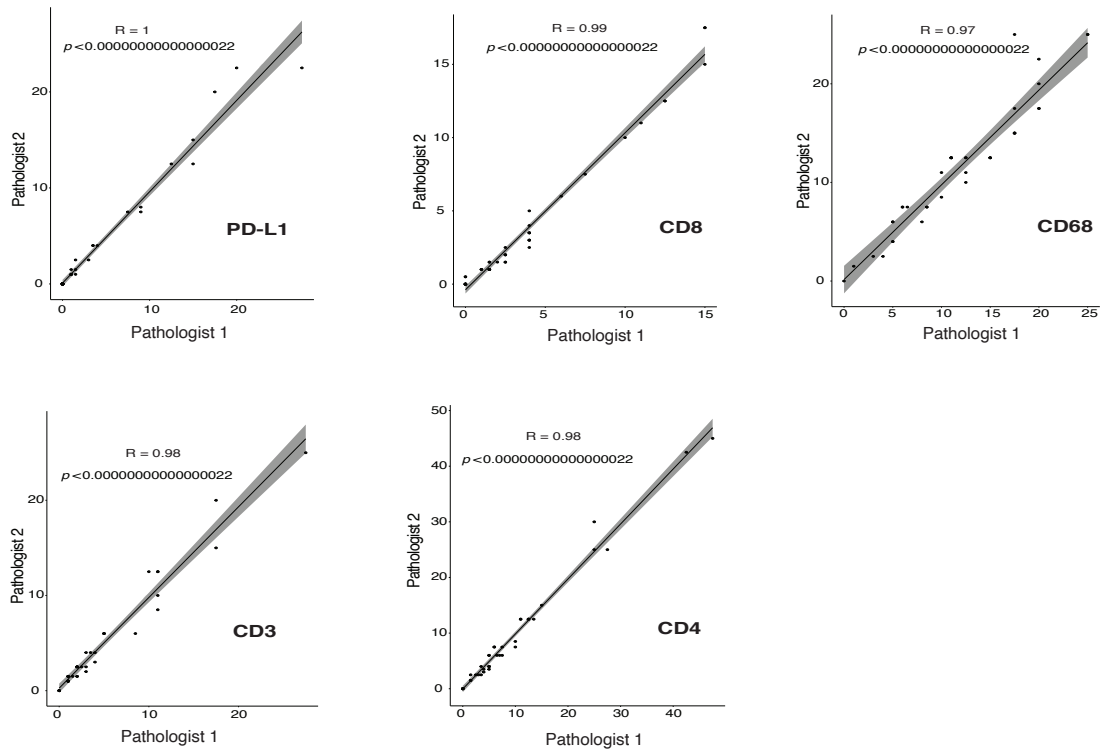


Supplementary Fig.S5. Predictive Genomic and Immune Biomarkers for CNS versus non-CNS solid tumors (excluding haematological malignancies). (a) SNVs and (b) MS-indel burden were similar for CNS and non-CNS solid tumors. Responders and non-responders stratified by (d) SNV and (e) MS-indel burden and tissue type (Green- Non-CNS solid tumors, blue- CNS tumours). (e) CD8 and (f) PDL1 were significantly higher for non-CNS solid tumors. Responders had higher levels of (g) CD8 T-cell infiltration and (h) PD-L1 staining as compared to non-responders in all tumours (Green- Non-CNS solid tumors, blue- CNS tumours). Representative images from non-CNS solid tumours, all of which demonstrated (i) high CD8 and (j) PD-L1 expression (20X). All immunohistochemistry was analysed by two independent pathologists. For all box-plots for responders and non-responders, data are represented as median +/- interquartile range. For statistical significance in comparing responders and non-responders, the Wilcoxon-Mann-Whitney test was used. All p values are 2-sided.

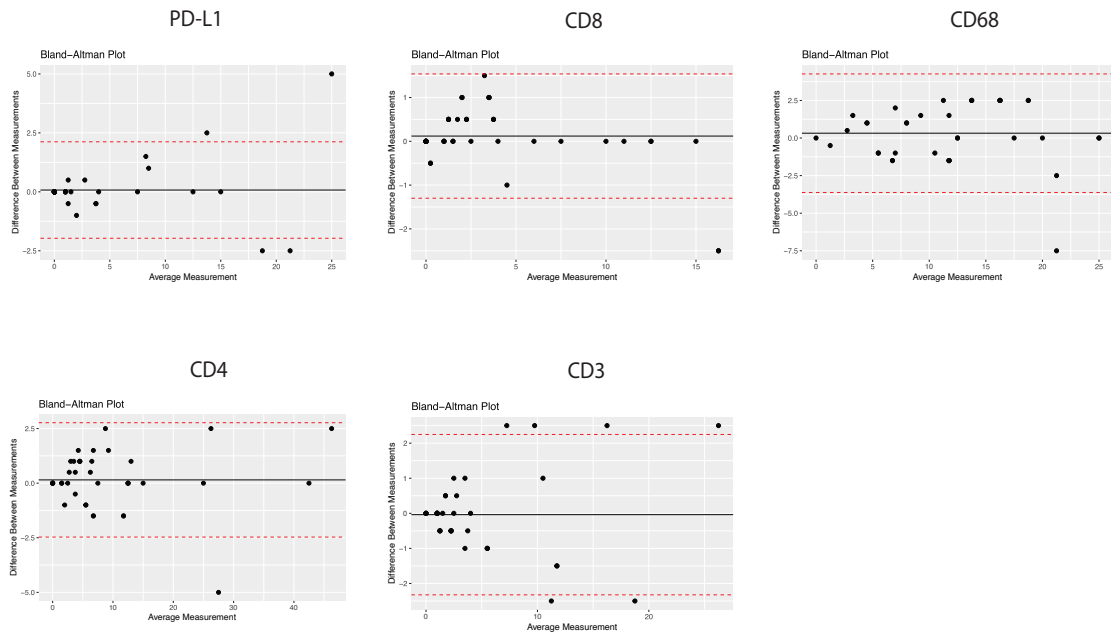


Supplementary Fig.S6. (A) TCGA glioma dataset demonstrated 34 tumors (6.8%) with TMB >5 mutations/Mb. **(B)** Extreme mutation burden in replication-repair deficient (RRD) glioma responders (n=21) as compared to non-responders (n=10) and adult hypermutant gliomas (n=34). **(C)** High MS-indel burden in replication-repair deficient (RRD) gliomas (responder: n=21; non-responder: n=10) as compared to adult hypermutant gliomas (n=34). For statistical significance in comparing responders and non-responders, the Wilcoxon-Mann-Whitney test was used. All p values are 2-sided.

a

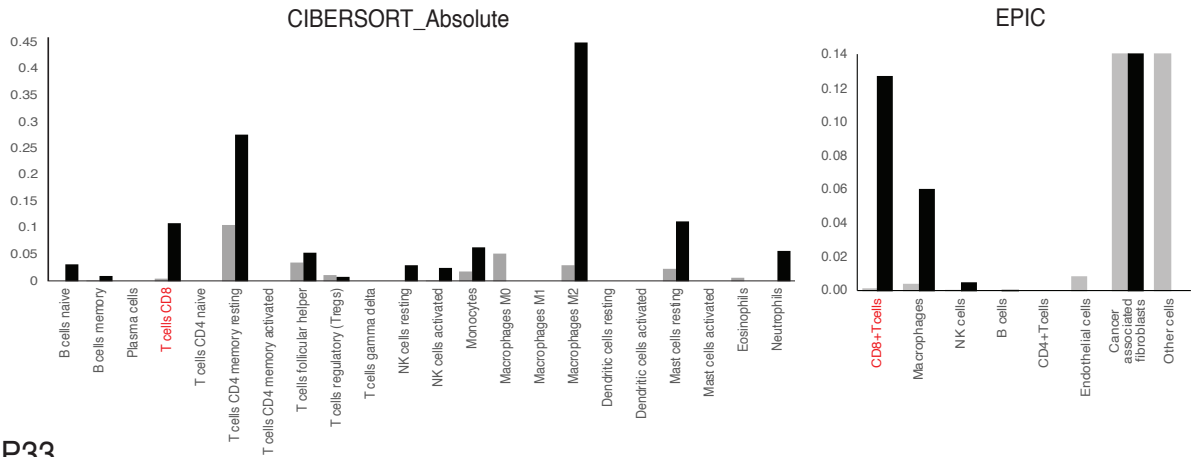


b

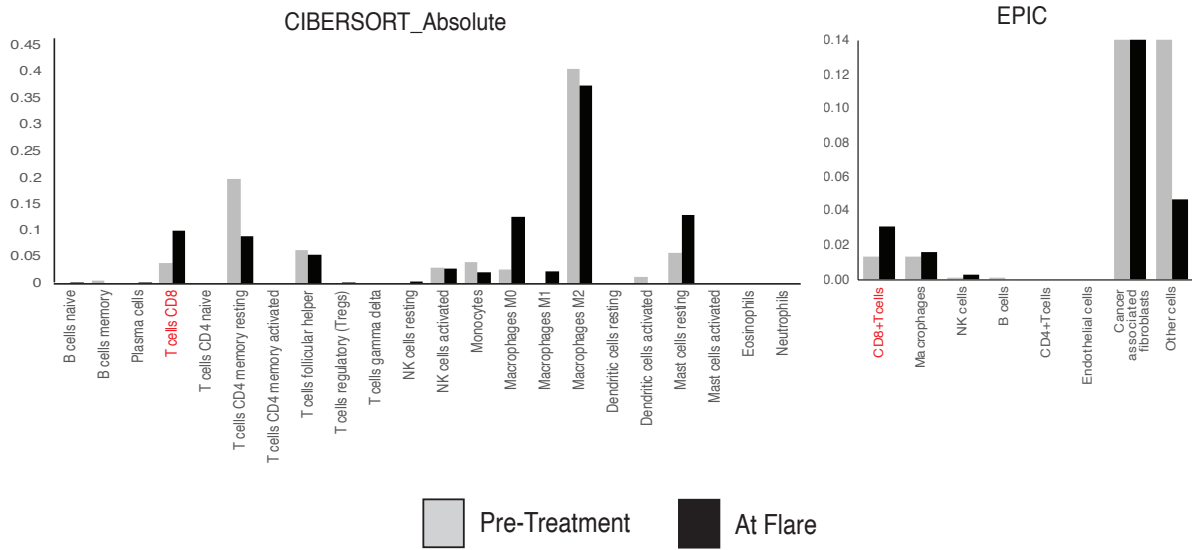


Supplementary Fig.S7. Concordance between immunohistochemical analyses and interpretation between two independent pathologists (CH/NA and OK) shown using **(a)** Spearman's rank correlation and **(b)** Bland-Altman plots. (Red dotted lines: 95% confidence intervals)

a. P31

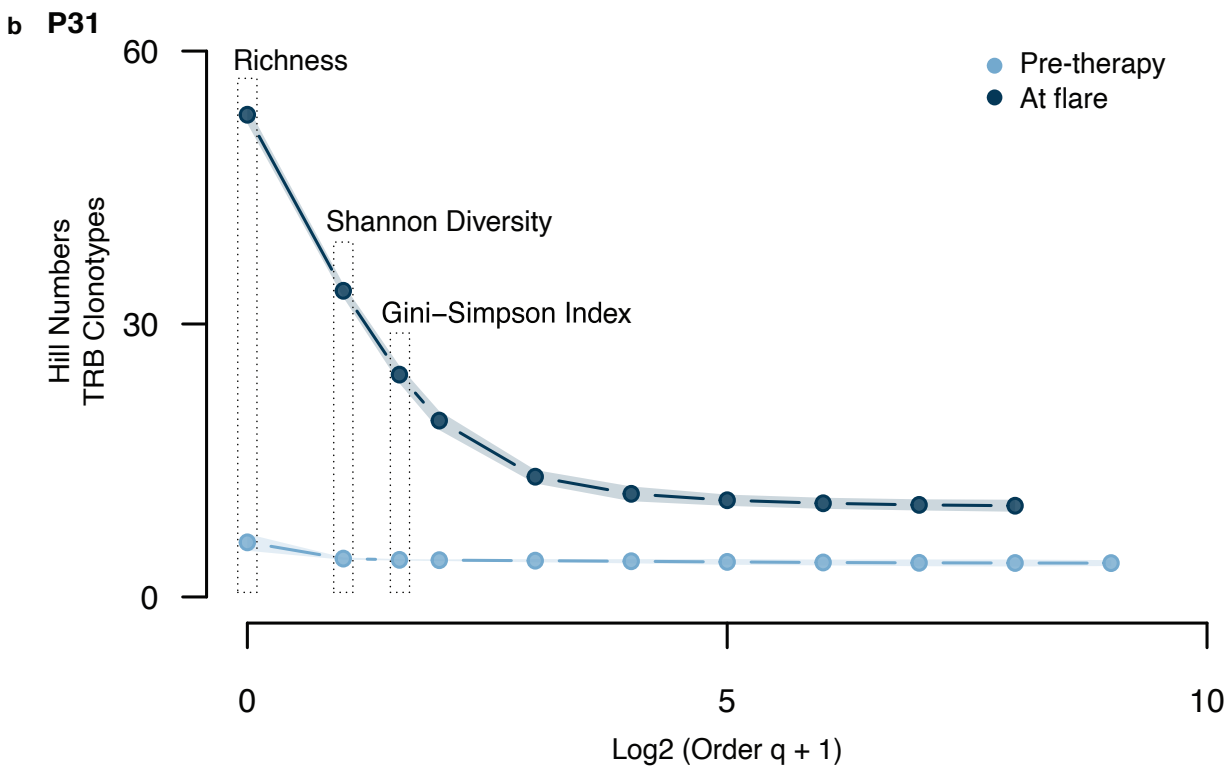
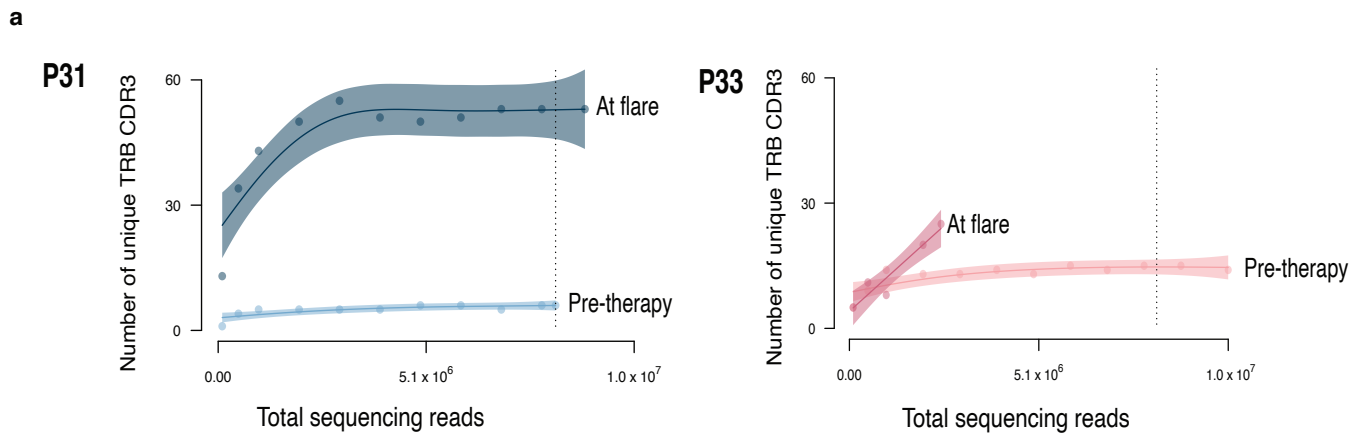


b. P33



Pre-Treatment At Flare

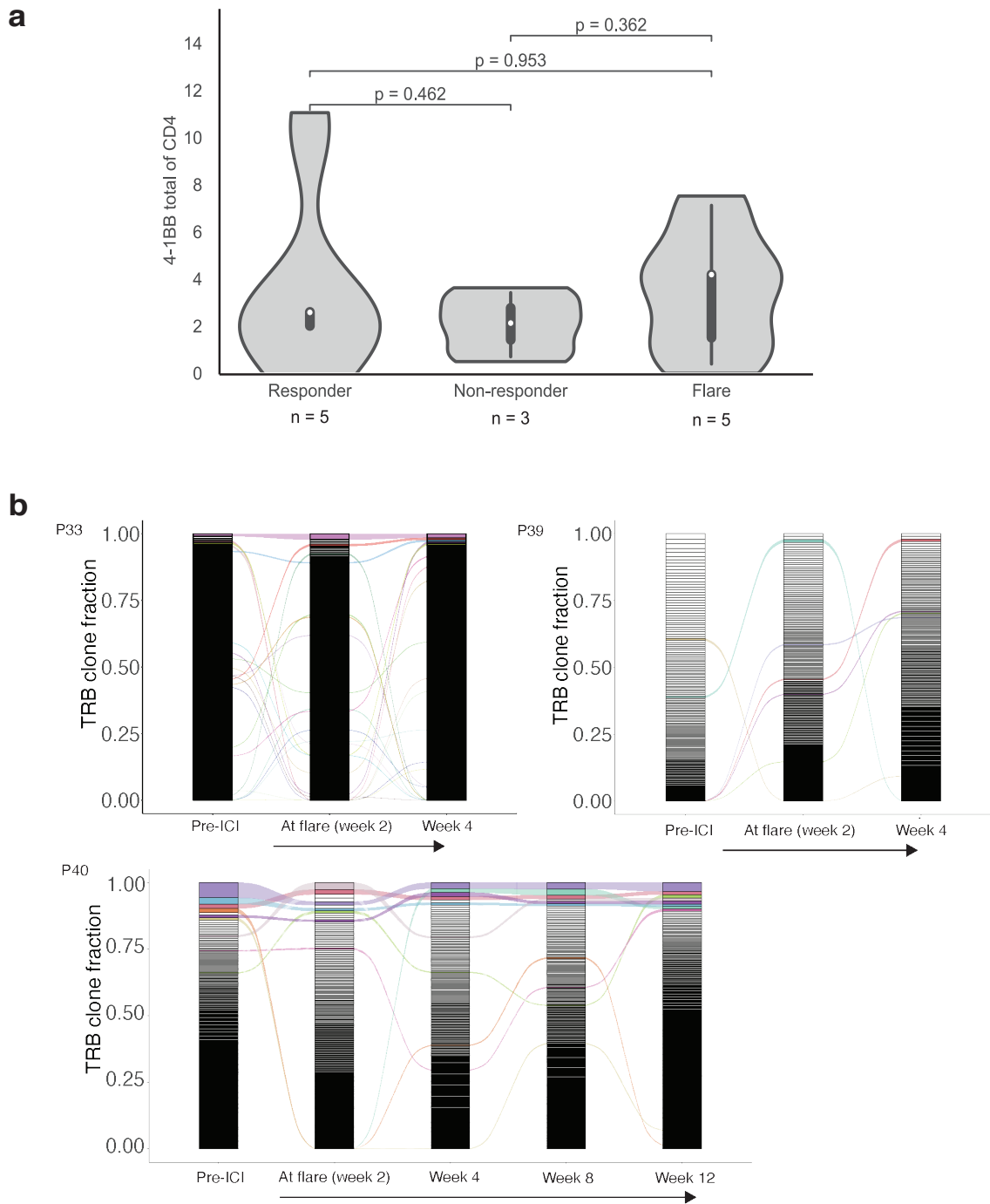
Supplementary Fig.S8. Immune inference of tumor microenvironment at baseline and at flare. Deconvolution analyses of tumor samples of two patients (a) P31 and (b) P33 using CIBERSORT_Absolute and EPIC (CD8+ T-cells are highlighted in red). (c) and (d) Same tumors demonstrating the actual abundance of all cell populations.



c P33

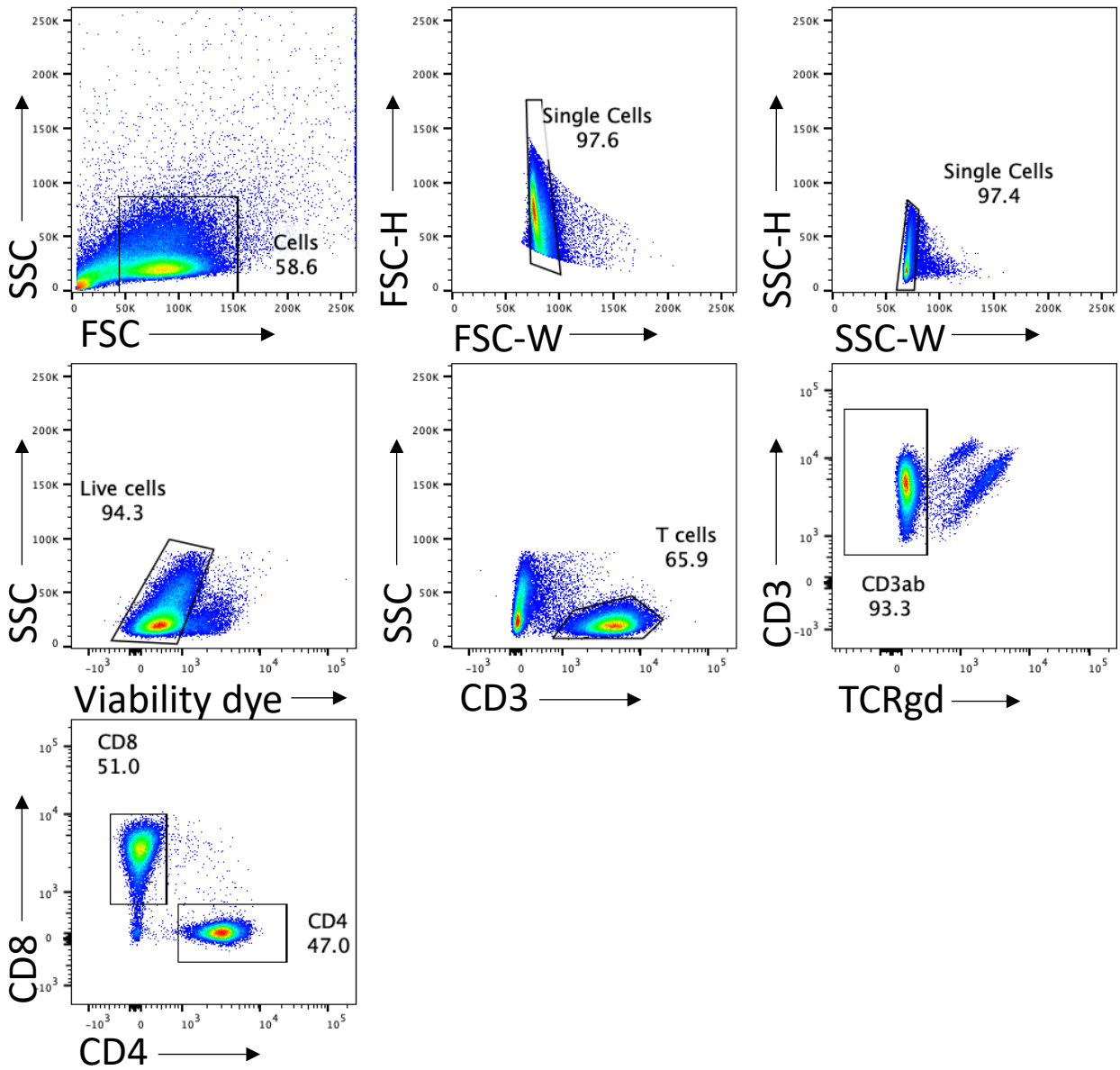
T-cell Receptor	Clone Count	aaSeqCDR3	IEDB	VDJdb	McPAS-TCR
TRB	1414	CASSQGGWDR_PTAYQETQYF	Not reported	Not reported	Not reported
TRB	1034	CATSVQGYNEQFF	Not reported	Not reported	Not reported
TRB	785	CASSPGGLTTGNTIYF	Not reported	Not reported	Not reported

Supplementary Fig.S9. (a) Sequencing reads for two patients at diagnosis and at time of flare (Data are presented as mean values \pm SEM). **(b)** TRB richness and diversity measures at flare compared to baseline for P31 (sequencing had reached saturation for both samples at pre-therapy and at flare). **(c)** Complementary-determining regions (CDR3) sequences of the major three clonotypes detected at flare in P33 (TRB: T cell receptor beta).



Supplementary Fig.S10. Immune responses in peripheral blood at flare. (a) 4-1BB+ CD4+ T-cells in blood from responders without flare, non-responders and flare. For the box-plots, data are represented as median +/- interquartile range. For statistical significance in comparing responders and non-responders, the Wilcoxon-Mann-Whitney test was used. All p values are 2-sided. **(b)** TRB clonotypes were tracked in 3 patients at baseline, time of flare, and following ICI continuation. Each box represents a distinct TRB clonotype. Clonotypes detected multiple time-points are color-coded and tracked in serial samples over time.

Flow Cytometry Gating Strategy



Supplementary Fig. S11. Gating strategy for flow cytometry utilized in the index study.

